CrystEngComm

ROYAL SOCIETY
OF CHEMISTRY

PAPER
Jannis Wehmeier and Markus Haase
Na$_{1.5-x/2}$Sr$_x$Gd$_{1.5-x/2}$F$_6$ nanocrystals ($0 \leq x \leq 1$): growth, size
control and shell formation on β-NaCeF$_4$:Tb core particles

Na$_{1,5-\frac{x}{2}}$Sr$_x$Gd$_{1,5-\frac{x}{2}}$F$_6$ nanocrystals (0 ≤ *x* ≤ 1): growth, size control and shell formation on β-NaCeF$_4$:Tb core particles†

Jannis Wehmeier [iD] and Markus Haase [iD] *

Na$_{1,5-\frac{x}{2}}$Sr$_x$Gd$_{1,5-\frac{x}{2}}$F$_6$ is an interesting shell material for β-NaREF$_4$ particles of the lighter lanthanides (RE = Ce, Pr, Nd), as variation of its strontium content *x* allows to vary its lattice parameters and match those of the core material. It crystallizes in the hexagonal gagarinite structure (NaCaYF$_6$) which is closely related to the hexagonal structure of β-NaREF$_4$, known from the upconversion host lattices β-NaYF$_4$ and β-NaGdF$_4$. Here, we studied the formation of **Na$_{1,5-\frac{x}{2}}$Sr$_x$Gd$_{1,5-\frac{x}{2}}$F$_6$** nanocrystals over the entire range 0 ≤ *x* ≤ 1. Heating of a solution of the metal oleates in oleic acid/octadecene in the presence of NH$_4$F results in the formation of small (≈3 nm) particles as the first product. For *x* ≤ 0.2, these particles mainly consist of the hexagonal gagarinite phase whereas for *x* > 0.2 most particles crystallize in a cubic lattice resembling the structure of α-NaGdF$_4$. Further heating at 320 °C leads to dissolution of the cubic phase and formation of larger particles of the hexagonal phase. Both the time required for complete dissolution as well as the final size of the **Na$_{1,5-\frac{x}{2}}$Sr$_x$G$_{1,5-\frac{x}{2}}$F$_6$** particles systematically grows with increasing strontium content *x*, showing that high values of *x* decrease the number of hexagonal seeds formed. The lattice parameters of the hexagonal phase are found to increase linearly with *x* and become, for high values of *x*, similar to those of the hexagonal phase of NaCeF$_4$, NaPrF$_4$, and NaNdF$_4$. Small particles of the cubic phase of NaGdSrF$_6$ are shown to be suitable precursors to form a gagarinite shell on β-NaCeF$_4$:25% Tb particles.

1 Introduction

Doped and undoped NaGdF$_4$ nanocrystals are widely investigated owing to their interesting magnetic and optical properties. Applications of these nanocrystals have been proposed in the fields of magnetic resonance imaging (MRI),[1–7] multimodal labeling and imaging,[8–17] drug delivery,[18–22] photovoltaics[23–27] and security inks.[28–30] Usually, the particles are prepared in the hexagonal phase, known as the β-NaGdF$_4$ phase, which is the thermodynamically most stable phase of the bulk material at low temperatures. The exact crystal structure of the hexagonal phase of NaGdF$_4$ (RE = rare earth) is a matter of a long-lasting debate and has been assigned to the space groups *P*6$_3$/*m* or *P*6̄.[31] Recently, large single crystals of β-NaGdF$_4$ could be successfully grown by the Czochralski method and the structures of these crystals have been shown to belong to *P*6$_3$/*m*.[32] The structure of β-NaGdF$_4$ is therefore directly related to the structure of the naturally occurring

mineral Gagarinite, NaCaYF$_6$,[33] which crystallizes in the same space group.[34–39] In fact, if one half of the Ca^{2+} ions in gagarinite is replaced by sodium ions and the other half by Y^{3+} ions, the hexagonal phase of NaYF$_4$ is obtained which can also be written as Na(Na$_{0.5}$Y$_{0.5}$)YF$_6$ or Na$_{1.5}$Y$_{1.5}$F$_6$. Partial replacement is also possible leading to compositions given by Na$_{1,5-\frac{x}{2}}$Ca$_x$Y$_{1,5-\frac{x}{2}}$F$_6$, where *x*, the degree of substitution, ranges from *x* = 0 for β-NaYF$_4$ to *x* = 1 for gagarinite. The doping of NaREF$_4$ nanocrystals with Ca^{2+} ions has in fact already been investigated by several groups, in most cases however, without reference to the gagarinite structure.[40–57] Successful incorporation of Sr^{2+} ions in the lattice of β-NaREF$_4$ nanocrystals has also been reported, but only with comparatively low amounts of Sr^{2+} (*x* ≤ 0.33).[41,58,59]

The cubic high temperature phase of (bulk) NaYF$_4$, known as α-NaYF$_4$, crystallizes in the space group *Fm*3*m*. The structure is easily derived from the structure of CaF$_2$ by randomly substituting half of the Ca^{2+} ions by Na$^+$ ions and the other half by Y^{3+} ions.[60] Partial substitution of the calcium ions therefore results in compositions given by Na$_{1-x}$Ca$_{2x}$Gd$_{1-x}$F$_4$ where 0 ≤ *x* ≤ 1. Since the latter compositions may alternatively be written as Na$_{1,5-\frac{x}{2}}$Sr$_x$Gd$_{1,5-\frac{x}{2}}$F$_6$ with 0 ≤ *x* ≤ 3, the hexagonal and the cubic phase can be described with the same chemical formula. When large single crystals of CaF$_2$

Inorganic Chemistry I, Universität Osnabrück, Osnabrück, Germany.
E-mail: markus.haase@uos.de

This journal is © The Royal Society of Chemistry 2020

are doped with RE^{3+} ions, high dopant concentration of up to 40% RE^{3+} can be achieved although co-doping with Na^+ ions is often omitted.[61] In this case, charge compensation is provided by additional fluoride ions, yielding compositions given by $Ca_{1-x}RE_xF_{2+x}$. The crystal structure of such rare earth doped CaF_2 and SrF_2 crystals has been thoroughly investigated, because single crystals of the materials represent an important class of solid state laser materials.[62] It has been shown that the rare earth ions form clusters in the crystal lattice and that cluster formation strongly affects the optical properties of the laser crystals.[63] The cubic phase of $NaYF_4$, on the other hand, is known to form solid solutions with varying compositions and is therefore better given by $\alpha\text{-}Na_{1-z}YF_{4-z}$. According to the phase diagram of the $NaF\text{-}YF_3$ bulk system, z ranges from 0 to 4/9.[64,65]

The two phases of $NaREF_4$ also play an important role in the synthesis of $\beta\text{-}NaREF_4$ particles with narrow size distribution. In the synthesis of $\beta\text{-}NaYF_4$ nanocrystal, for instance, it is generally observed that a large number of small particles of the metastable cubic phase ($\alpha\text{-}NaYF_4$) are formed as the first product at early stages of the synthesis. In addition, a much smaller number of particles of the hexagonal phase ($\beta\text{-}NaYF_4$) nucleate, either together with the $\alpha\text{-}NaYF_4$ particles or during further heating. In the following stages of the synthesis taking place at high temperature, the $\alpha\text{-}NaYF_4$ particles dissolve and the material released is consumed by the $\beta\text{-}NaYF_4$ particles which grow in size. This transfer of material from the $\alpha\text{-}NaYF_4$ to the $\beta\text{-}NaYF_4$ particles shows that the metastable cubic phase must have a higher solubility in oleic acid/octadecene solution than the hexagonal phase. The narrow size distribution of the final $\beta\text{-}NaYF_4$ particles indicates that their growth took place under the condition of monomer supersaturation. The $\alpha\text{-}NaYF_4$ particles are the origin of the monomer supersaturation, as $\beta\text{-}NaYF_4$ particles grown in the absence of $\alpha\text{-}NaYF_4$ particles form a broad size distribution.[66] Obviously, the large number of better soluble $\alpha\text{-}NaYF_4$ particles generates a monomer concentration so high that the less soluble $\beta\text{-}NaYF_4$ particles grow with focusing of their size distribution.[67,68] In a similar way, $\beta\text{-}NaGdF_4$ and other $\beta\text{-}NaREF_4$ particles with narrow size distribution can be prepared by using particles of the cubic phase as precursor.

In the work presented here we studied the synthesis of $\beta\text{-}Na_{1.5-\frac{x}{2}}Sr_xGd_{1.5-\frac{x}{2}}F_6$ particles, also starting from small $\alpha\text{-}Na_{1.5-\frac{x}{2}}Sr_xGd_{1.5-\frac{x}{2}}F_6$ particles as precursor. Different compositions x were investigated including the highest value $x = 1$ which corresponds to the gagarinite structure, and we found the strontium amount x to have a central role in the nucleation and growth of the nanoparticles. While high strontium concentrations prohibit the direct formation of pure $\beta\text{-phase}$ $NaSrGdF_6$ ($x = 1$), a composition close to the gagarinite structure ($x = 0.979$) was achieved by a core/shell approach. Additionally, $\alpha\text{-}Na_{1.5-\frac{x}{2}}Sr_xGd_{1.5-\frac{x}{2}}F_6$ particles were found to be a suitable precursor material to form a shell of gagarinite on $\beta\text{-}NaREF_4$ core particles of the lighter lanthanides such as Tb^{3+} doped $\beta\text{-}NaCeF_4$ nanoparticles.

2 Experimental

2.1 Chemicals and materials

Purified oleic acid (90%, Fisher), 1-octadecene (90%, Alfa Aesar), sodium oleate (82%, Sigma Aldrich), strontium acetate (99%, Sigma Aldrich) and ammonium fluoride (98%, Alfa Aesar) were used as received. Gd_2O_3 (99.9%, Intematix) was used to prepare anhydrous gadolinium acetate by the procedure described previously for other rare earth acetates.[69]

2.2 Synthesis of $Na_{1.5-\frac{x}{2}}Sr_xGd_{1.5-\frac{x}{2}}F_6$ nanocrystals

20 ml of oleic acid (OA) and 20 ml of 1-octadecene (ODE) were combined in a 100 ml three-neck round bottom flask and connected to a reflux condenser, heating mantle and temperature controller. At room temperature, $4x$ mmol strontium acetate ($0.2 \le x \le 1$), $6-2x$ mmol anhydrous gadolinium acetate and $14-2x$ mmol sodium acetate were added to the OA/ODE solvent. The stirred mixture was heated to 100 °C under vacuum and left at this temperature for one hour. The apparatus was refilled with nitrogen and the clear solution heated to 300 °C. Heating was stopped after 60 minutes and the mixture was allowed to cool to 100 °C. To remove the acetic acid released during the heating step at 300 °C, vacuum was applied again and the solution degassed for 30 minutes at 100 °C. Thereafter, 1.185 g (32 mmol) of dry NH_4F powder were added at 100 °C under nitrogen counter flow. To remove air, the vessel was subjected three times to a short vacuum (5–10 s) and refilled with nitrogen. The stirred mixture was then heated to 200 °C. After 45 minutes at 200 °C, the temperature was raised to 320 °C and the solution kept at this temperature for different times ranging from 5 minutes to 12 hours. From time to time, 5 ml samples were drawn at 320 °C with a syringe. The samples were immediately quenched in twice the volume of ethanol, resulting in precipitation of the particles. After centrifugation, the precipitate was re-suspended in 15 ml of hexane and again centrifuged to separate the hexane solution containing the particles from the NaF byproduct. The particles were again precipitated with 30 ml of ethanol, separated by centrifugation and dried over night in air.

2.3 Synthesis of $NaCeF_4$:Tb nanocrystals

$NaCeF_4$:Tb nanocrystals were prepared by following a literature procedure for $NaCeF_4$.[70] In brief, 3 mmol of cerium oleate, 1 mmol of terbium oleate, and 10 mmol of sodium oleate in a 100 ml three-neck round bottom flask were combined with 10 ml of oleic acid, 10 ml of oleyl amine, and 20 ml of 1-octadecene (ODE). The metal oleates were dissolved and the solvent degassed by stirring the mixture at 100 °C for one hour under vacuum. After switching to nitrogen atmosphere, 815 mg (22 mmol) of dry NH_4F powder were added at 100 °C. To remove air, the flask was subjected three times to a short vacuum (5–10 s) and refilled with nitrogen. The stirred mixture was then heated for 60 minutes at 290 °C. After cooling to room temperature, the nanocrystals were precipitated by

adding 50 ml of ethanol and purified as described above for the $Na_{1.5-\frac{x}{2}}Sr_xGd_{1.5-\frac{x}{2}}F_6$ nanocrystals.

2.4 Synthesis of core/shell nanocrystals with a shell of Gd, Sr-gagarinite (NaSrGdF$_6$)
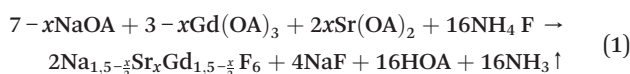
For the synthesis of core/shell particles, 20 ml of oleic acid (OA) and 20 ml of 1-octadecene (ODE) were added to 4 mmol of strontium acetate, 4 mmol of anhydrous gadolinium acetate and 12 mmol of sodium acetate in a 100 ml three-neck round bottom flask. The mixture was first degassed for one hour by heating at 100 °C under vacuum, thereafter refilled with nitrogen and heated at 300 °C for 90 minutes. After cooling to 100 °C vacuum was applied again and the solution degassed for 30 minutes at 100 °C to remove the acetic acid released at 300 °C. Thereafter, the apparatus was again switched to nitrogen atmosphere and either 0.57 mmol of $Na_{1.5-\frac{x}{2}}Sr_xGd_{1.5-\frac{x}{2}}F_6$ particles or 0.86 mmol of NaCeF$_4$:Tb particles were added at 100 °C together with 0.889 g (24 mmol) of dry NH$_4$F powder. To remove air, the vessel was subjected three times to a short vacuum (5–10 s) and refilled with nitrogen. The stirred mixture was then heated to 200 °C under nitrogen atmosphere. After 45 minutes at 200 °C, the temperature was raised to 320 °C and the solution heated at this temperature for 45 minutes. After cooling to room temperature, the core/shell nanocrystals were precipitated by adding 50 ml of ethanol and purified as described above for the $Na_{1.5-\frac{x}{2}}Sr_xGd_{1.5-\frac{x}{2}}F_6$ nanocrystals.

2.5 Particle characterization

For transmission electron microscopy, a JEOL JEM 2100 TEM was used. The TEM was operated at 200 kV and equipped with a LaB$_6$ cathode. Particle size histograms were derived from TEM images using the software Pebbles. X-ray powder diffraction (XRD) data were recorded with a Panalytical Empyrean diffractometer using Bragg–Brentano geometry, Cu K-α radiation and a step size of 0.039° 2θ. Profex and Fullprof software were used for Rietveld analysis of the XRD data and to determine the phase composition, respectively. The atomic composition of the nanoparticles was analysed with an Axios X-ray fluorescence spectrometer (Panalytical). Luminescence spectra of nanoparticle powders were measured with a Fluorolog-3 spectrofluorometer (Horiba).

3 Results and discussion

$Na_{1.5-\frac{x}{2}}Sr_xGd_{1.5-\frac{x}{2}}F_6$ nanocrystals were prepared at temperatures above 200 °C by the reaction of solid ammonium fluoride with a solution of sodium oletate, gadolinium oleate, strontium oletate in oleic acid/1-octadecene:

$$7-xNaOA + 3-xGd(OA)_3 + 2xSr(OA)_2 + 16NH_4F \rightarrow$$
$$2Na_{1.5-\frac{x}{2}}Sr_xGd_{1.5-\frac{x}{2}}F_6 + 4NaF + 16HOA + 16NH_3\uparrow \quad (1)$$

Different molar ratios of strontium to gadolinium and sodium were employed in the synthesis and the NaF byproduct

was removed during work-up (see Experimental section for details). X-ray powder diffraction shows that particles of the hexagonal phase (β-phase) of $Na_{1.5-\frac{x}{2}}Sr_xGd_{1.5-\frac{x}{2}}F_6$ are formed at 200 °C for values of $x \leq 0.25$. These particles have a very small size of only 2–3 nm. For $x \geq 0.25$, the samples heated at 200 °C consist predominantly of very small particles of the cubic phase (α-phase) $Na_{1.5-\frac{x}{2}}Sr_xGd_{1.5-\frac{x}{2}}F_6$ (Fig. 1).

When the temperature is increased to 320 °C, the particles of the cubic phase dissolve and larger particles of the hexagonal phase are formed. The XRD data in Fig. 1 and 2 also show that the dissolution time strongly depends on x, *i.e.*, the amount of strontium in the synthesis: when only small amounts of strontium are used ($x = 0.5$), complete conversion to the hexagonal phase is observed already after 6 minutes at 320 °C. For $x = 1$, on the contrary, 60% of the particles remained in the cubic phase even after 12 hours of heating at 320 °C. In fact, complete conversion to the α-phase was only observed for $0 \leq x < 0.8$.

TEM images and particle size histograms of the resulting particles are shown in Fig. 3 and S1,† respectively. The figures show that narrow, monomodal size distributions are obtained for $0 \leq x \leq 0.75$ and bimodal size distributions for $x = 0.8$ and $x = 1$. For $x = 1$, the TEM image and the size histogram display a large number of small particles. These particles consist of the cubic phase, as confirmed by the XRD data of the sample (Fig. 2) showing that the peaks of the cubic phase are broader than those of the hexagonal phase. For $x = 0.8$ the number of small particles is very low and the sample mainly consists of larger particles of the hexagonal phase. The mean size of the particles of the hexagonal phase is 57 nm for $x = 1$, 23 nm for $x = 0.8$ and between 7 nm and 14 nm
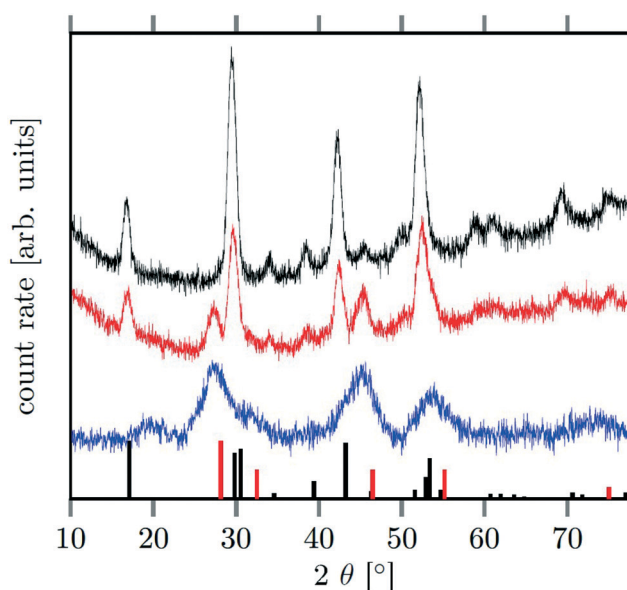

Fig. 1 XRD data of $Na_{1.5-\frac{x}{2}}Sr_xGd_{1.5-\frac{x}{2}}F_6$ particles with $x = 0.5$. Particles formed after heating for 45 min at 200 °C (blue), after reaching 320 °C (red), and after heating for 6 min at 320 °C (black). The vertical lines correspondent to the reference patterns of α-NaGdF$_4$ (red, ICSD-# 77099) and β-NaGdF$_4$ (black, ICSD-# 415868) respectively.
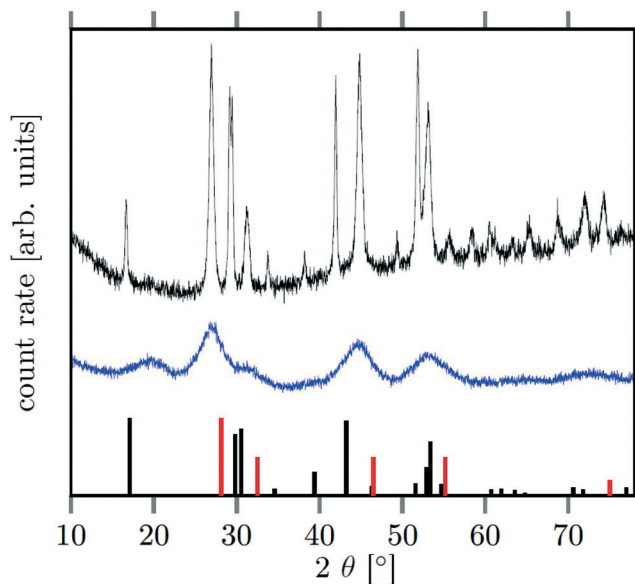
Fig. 2 XRD data of $Na_{1.5-\frac{x}{2}}Sr_xGd_{1.5-\frac{x}{2}}F_6$ particles with $x = 1$. Particles formed after heating for 45 min at 200 °C (blue), and after heating for 720 min at 320 °C (black). The vertical lines correspondent to the reference patterns of α-NaGdF$_4$ (red, ICSD-# 77099) and β-NaGdF$_4$ (black, ICSD-# 415868) respectively.

Fig. 3 TEM-images of β-$Na_{1.5-\frac{x}{2}}Sr_xGd_{1.5-\frac{x}{2}}F_6$ nanoparticles with (a) x = 0.2 (b) x = 0.4 (c) x = 0.5 (d) x = 0.6 (e) x = 0.7 (f) x = 0.75 (g) x = 0.8 (h) x = 1. For x = 1, complete dissolution of the particles of the cubic phase was not achieved. A small amount of the cubic phase is also contained in the sample with x = 0.8.

for $x \leq 0.75$. In all cases, the particles of the hexagonal phase display narrow size distributions, indicating that the particles have grown under the condition of monomer supersaturation.

The observation that the α-phase particles dissolve whereas the β-phase particles grow in size, in fact indicates that the solubility of the α-phase is higher. In mixtures containing a large number of α-phase particles but a small number of β-phase particles, the high solubility of the α-phase particles can therefore be expected to produce a higher monomer concentration in solution than the β-phase particles would do in the absence of α-phase particles. The β-phase particles in the mixture therefor grow under monomer supersaturation, causing their narrow size distribution.

The large mean size of the hexagonal particles for $x \geq 0.8$ already shows that a high strontium content decreases the number of β-phase seeds nucleating in solution. In Fig. 4 the observed final particle size is plotted against the strontium content used in the synthesis. The figure shows that the size increases systematically with the strontium content given by the degree of substitution x. Obviously, the strontium ions suppress the nucleation of β-phase seeds and favor the formation of the cubic phase. This is not unexpected, since the cubic phase of bulk SrF$_2$ is the thermodynamically most stable phase at low temperature whereas the cubic phase of bulk NaGdF$_4$ is only metastable. Wang *et al.* in fact observed that doping of α-NaYF$_4$:Eu particles with Sr reduces their mean particle size, indicating that the strontium ions facilitate the nucleation of α-phase seeds. In our samples, the decrease of the number of the β-phase seeds not only results in larger sizes of the final particles but also in a strong increase of the
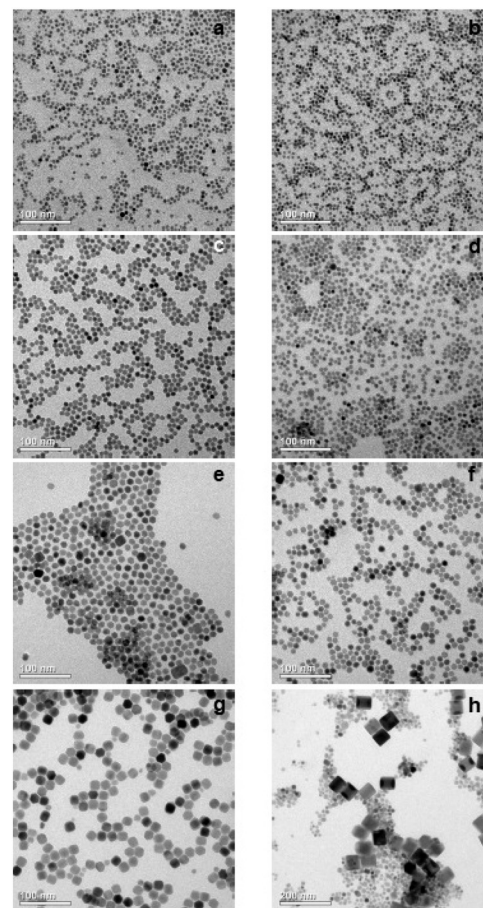
time required to convert all particles to the hexagonal phase. This is shown in Fig. 5 where the time required to dissolve
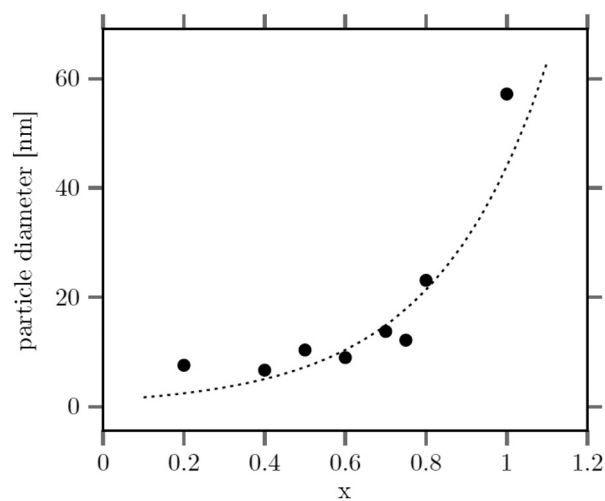

Fig. 4 Dependence of the size of β-$Na_{1.5-\frac{x}{2}}Sr_xGd_{1.5-\frac{x}{2}}F_6$ nanoparticles on their strontium content x.
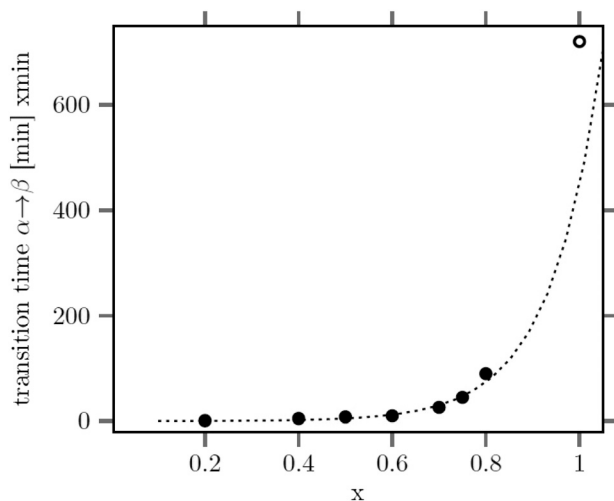
Fig. 5 Time of heating at 320 °C required to dissolve all particles of the cubic phase *versus* their strontium content *x*. For *x* = 1, even 720 min at 320 °C are not sufficient for complete dissolution.

Fig. 6 Strontium content *x* (black) and sodium/gadolinium ratio (red) of the final nanoparticles, as determined by XRF, plotted against the strontium content x used to the synthesis.

the α-phase particles is plotted against the strontium content *x*. The strong increase of the conversion time is probably not only caused by the decreasing number of β-phase seeds but also by a lower solubility of the α-phase particles with increasing strontium content. For any given strontium content *x*, however, the α-phase particles must be significantly better soluble than the corresponding β-phase particles with the same strontium content, because narrow size distributions are observed for all β-phase particles, independent of *x* (Fig. 3).

The strontium content *x* of the data points used in Fig. 4 and 5 were calculated from ratio of strontium to acetate (Sr/Gd) employed in the synthesis. From the chemical formula $Na_{1.5-\frac{x}{2}}Sr_xGd_{1.5-\frac{x}{2}}F_6$ it follows that this molar ratio is connected to the value of *x* by $x = 3(Sr/Gd)/[2 + (Sr/Gd)]$. To compare these values with the actual composition of the final particles, the sodium, strontium and gadolinium content of the particles was determined by X-ray fluorescence analysis (XRA). Fig. 6 displays the measured molar ratios of strontium to gadolinium, given as *x* values, as well as the molar ratios of sodium to gadolinium. The figure shows that the *x* values calculated from the XRA data agree well with those derived from the ratio of strontium to gadolinium employed in the synthesis. The ratio of sodium to gadolinium shows some scattering but is close to one in all samples, independent of the amount of strontium used. The first result proves that the strontium is completely incorporated into the particles whereas the second result shows that the different charge of the Sr^{2+} ions is compensated in our case by replacing sodium and gadolinium ions in the crystal lattice in equal numbers. This is expected from the compositions discussed in our introduction but in contradiction to results reported by others where charge compensation by fluoride ions was observed. A possible explanation for this discrepancy could be the different concentrations of fluoride ions used in the two experimental procedures or the different alkaline earth and rare earth sources.
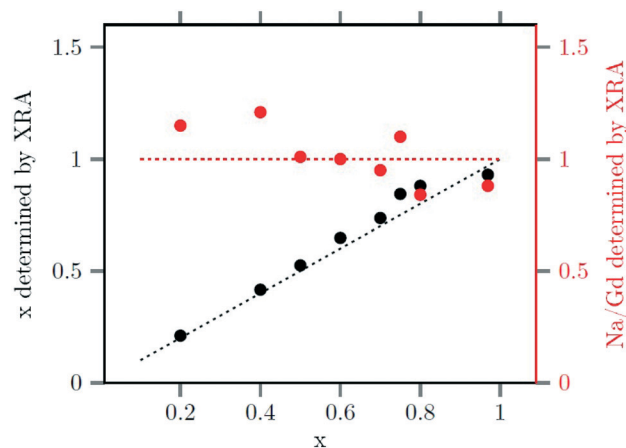
The successful incorporation of the Sr^{2+} ions can also be verified by Rietveld analysis of the X-ray powder diffraction data, since the radius of Sr^{2+} ions (132 pm) is larger than the radius of sodium ions (116 pm) and the radius of Gd^{3+} ions (108 pm). This is in contrast to the analogue Ca, Gd-gagarinite, where the ionic radius of Ca^{2+} (114 pm) is very close to the average of the ionic radii of Na^+ and Gd^{3+} (112 pm), *i.e.*, the ions partially substituted by Ca^{2+}. The larger radius of Sr^{2+} results in an increase of the unit cell shifting the reflex positions to smaller 2θ values. In Fig. 7, the lattice parameters *a* and *c* of the hexagonal unit cell are plotted against the Sr^{2+} content of the nanocrystals, given by the degree of substitution *x*. A linear dependence is observed up to *x* ≤ 0.8 in accord with Vegard's law stating that the lattice parameters of a solid solution $A_{1-x}B_x$ vary linearly with x in first approximation. For *x* = 1, however, the increase of the lattice parameters is lower than expected. Note, that in this case complete dissolution of the cubic α-phase could not be
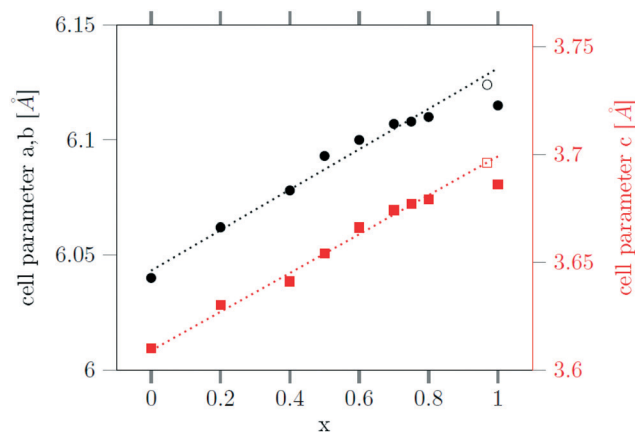

Fig. 7 Dependence of the lattice constants *a* (black) and *c* (red) of the hexagonal gagarinite phase on the strontium content *x* of the β-$Na_{1.5-\frac{x}{2}}Sr_xGd_{1.5-\frac{x}{2}}F_6$ nanoparticles.

achieved even after 12 hours of heating at 320 °C (Fig. 2). Moreover, the large particle sizes observed for $x \geq 0.8$ show that only a small number of seeds nucleate in this case. To increase the number of seeds available during the conversion, we heated the 3 nm α-NaGdSrF$_6$ particles (*i.e.*, particles with $x = 1$) in the presence of 10 nm β-Na$_{1.125}$Sr$_{0.75}$Gd$_{1.125}$F$_6$ particles (*i.e.*, $x = 0.75$) as additional seeds.

Seeds with $x = 0.75$ were chosen because this value of x corresponds to the most strontium rich composition for which complete conversion to the β-phase was achieved. Since we combined the α-NaSrGdF$_6$ particles and the β-Na$_{1.125}$Sr$_{0.75}$Gd$_{1.125}$F$_6$ seeds in molar ratio of 7 to 1, the nominal composition of the β-phase particles produced in this core/shell type synthesis is expected to be $x = 0.97$ $\left(x = \frac{1}{8} \cdot 0.75 + \frac{7}{8} \cdot 1.0\right)$. The XRD data of samples drawn at different reaction times (Fig. 8) show that this method results in a high degree of conversion to the β-phase. Rietveld analysis of the XRD data shows that heating at 320 °C for 90 minutes, 200 minutes and 720 minutes alters the phase composition from the initial molar ratio of 7 to 1 to a molar ratio of 0.19 to 1, 0.12 to 1, and 0.05 to 1, respectively. Thus, 200 minutes of heating at 320 °C dissolves already more than 98% of the initial amount of α-phase material. The degree of conversion to the β-phase is therefore significantly higher than in the absence of seed particles where 12 hours of heating at 320 °C dissolves only 40% of the α-phase material (Fig. 2). Since the remaining α-phase particles are significantly smaller than the β-phase particles, however, the number of α-phase particles is still comparatively high and the resulting size distribution is again clearly bimodal as shown by the TEM image and the particle size histogram in Fig. S3 and S5.† The phase compositions derived from the histograms, however, are in accord with the Rietveld analysis, when the different volumes of the particles are taken into account (Fig. S3†). The Rietveld analysis furthermore shows that the unit cell parameters of the hexagonal phase produced in this core/shell type experiment are the largest of all β-phase materials prepared in this work (Fig. 7, open symbol). This indicates that the β-Na$_{1.5-\frac{x}{2}}$Sr$_x$Gd$_{1.5-\frac{x}{2}}$F$_6$ particles contain, on average, a high amount of strontium in the crystal lattice, probably close to the expected composition of $x = 0.97$. Fig. 7 shows that the large unit cell parameters of these particles are in fact much better in accord with the linear dependence of the unit cell parameters observed for lower values of x. The figure also shows that the unit cell parameters of these particles are significantly larger than those of the 40 nm particles prepared in the absence of seed particles. Obviously, the 40 nm particles contain less Sr^{2+} than the particles prepared by the core/shell type synthesis, *i.e.*, they are partially depleted of Sr^{2+}. The Sr^{2+} not contained in the 40 nm particles must therefore be part of the cubic phase which did not dissolve despite 12 hours of heating at 320 °C. Such enrichment of Sr^{2+} in the cubic phase is in fact possible, as the cubic phase can contain significantly more Sr^{2+} than the hexagonal phase. This follows from the different compositional ranges of the two phases: as already mentioned in the introduction, both phases are given by Na$_{1.5-\frac{x}{2}}$Sr$_x$Gd$_{1.5-\frac{x}{2}}$F$_6$, but for the cubic phase $0 \leq x \leq 3$ whereas for the hexagonal $0 \leq x \leq 1$. Thus, if α-phase particles with $x = 1$ are heated at 320 °C with the aim to prepare (Sr, Gd)-gagarinite particles with $x = 1$, a mixture may form which consists of hexagonal phase β-Na$_{1.5-\frac{x}{2}}$Sr$_x$Gd$_{1.5-\frac{x}{2}}$F$_6$ particles with $x \leq 1$ and cubic phase α-Na$_{1.5-\frac{x}{2}}$Sr$_x$Gd$_{1.5-\frac{x}{2}}$F$_6$ particles with $x \geq 1$. The slow conversion observed for $x = 1$ probably indicates that the solubility of α-Na$_{1.5-\frac{x}{2}}$Sr$_x$Gd$_{1.5-\frac{x}{2}}$F$_6$ particles with a high strontium content of $x \geq 1$ is very low.

The lattice parameters of the β-phase particles with the highest strontium content are $a = 6.124$ Å and $c = 3.696$ Å. These values are very similar to the unit cell parameters of β-NaLaF$_4$ ($a = 6.18$ Å, $c = 3.83$ Å), β-NaCeF$_4$ ($a = 6.153$ Å, $c = 3.785$ Å), β-NaPrF$_4$ ($a = 6.13$ Å, $c = 3.75$ Å), and β-NaNdF$_4$ ($a = 6.109$ Å, $c = 3.716$ Å). This indicates that the 3 nm α-NaSrGdF$_6$ particles might be a suitable shell precursor for β-NaREF$_4$ core particles of the lighter lanthanides, provided that the β-NaREF$_4$ core particles have sufficiently low solubility to obtain narrow size distribution. This is interesting, because the cubic phase of NaLaF$_4$ decomposes to LaF$_3$ upon heating in oleic acid/octadecene.[70] Small α-NaLaF$_4$ particles can therefore not be used as shell precursor, although β-NaLaF$_4$ would be the most straightforward choice of shell material for core particles composed of β-NaCeF$_4$, β-NaPrF$_4$, β-NaNdF$_4$ or NaLaF$_4$:RE. In the next step, we therefore studied the use our 3 nm α-NaSrGdF$_6$ particles as precursor to grow a shell on 8 nm β-NaCeF$_4$: 25% Tb core particles. Again, the shell precursor and the core particles were combined in a molar ratio of 7 to 1. The TEM images in Fig. 9 show
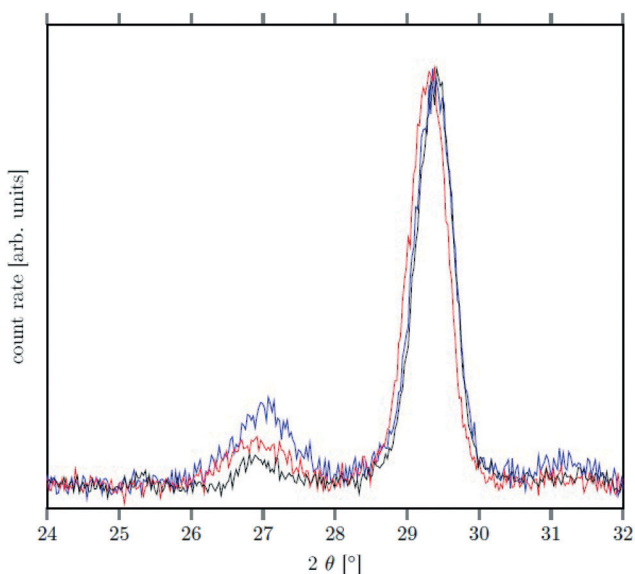

Fig. 8 XRD data of NaSrGdF$_6$@β-Na$_{1.125}$Sr$_{0.75}$Gd$_{1.125}$F$_6$ core/shell particles after heating at 320 °C for 90 min (black), 200 min (red) and 720 min (blue). The peak at $\approx 27°$ belonging to the α-phase is much less intense than the signal of the β-phase at $\approx 29.5°$ (compare also with Fig. 2).
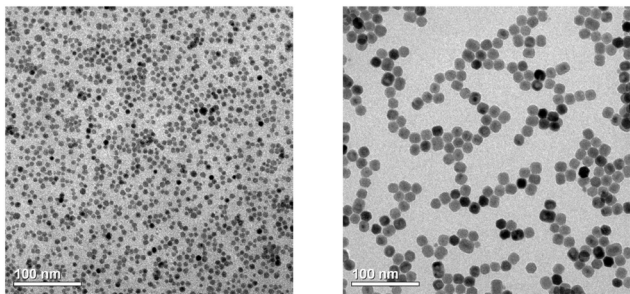
Fig. 9 TEM-images of NaCeF$_4$:Tb core (left) and NaCeF$_4$:Tb @NaSrGdF$_6$ core/shell particles (right).
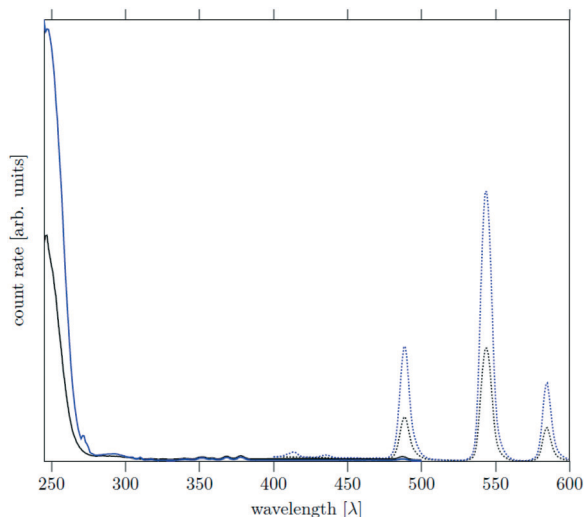

Fig. 10 Excitation and emission (dotted) spectra of NaCeF$_4$:Tb core (black) and NaCeF4:Tb@NaSrGdF$_6$ core/shell particles (blue). Excitation wavelength was 246 nm and emission wavelength 543 nm for both particle powders.

particles with a rather narrow size distribution and a size that has increased from 8 nm to 18 nm, *i.e.*, approximately by the expected factor of two.

We observe that the β-NaCeF$_4$: 25% Tb core particles consume the monomer released by the shell precursor much faster than the β-Na$_{1.125}$Sr$_{0.75}$Gd$_{1.125}$F$_6$ seeds: already after 45 minutes all α-NaSrGdF$_6$ particles have dissolved compared to >200 min required to dissolve >98% of these particles in the second case. This is also in accord with the narrower size distribution of the resulting NaCeF$_4$: 25% Tb@NaSrGdF$_6$ core/shell particles (Fig. S4†). As expected for a core/shell structure, the resulting NaCeF$_4$: 25% Tb@NaSrGdF$_6$ particles consist only of the hexagonal phase and display improved luminescence properties compared to the NaCeF$_4$: 25% Tb coreparticles.

The core as well as the core/shell particles display a strong absorption band in the UV region due to the optically allowed 4f–5d transitions of cerium. Similar to other Ce, Tb co-doped materials, excitation of the cerium ions at 246 nm results in energy transfer from cerium to terbium accompanied by strong quenching of the Ce^{3+} emission between 400 nm and 450 nm. Relaxation of the excited terbium ions leads to strong emission bands at 490 nm, 545 nm and 585 nm which correspond to the $^5D_4$–^7F_J transitions (J = 4, 5, 6) of Tb^{3+}. The emission spectra in Fig. 10 show that the core and core/shell particles display the same emission bands, but the emission of the core/shell particles is approximately 2.5 times more intense. This shows that the shell reduces energy transfer to and quenching of the luminescence at the particle surface.

As expected, the increase is less pronounced than in the case of NIR emitting dopants, since the UV-vis transitions of Ce^{3+} and Tb^{3+} are less easily quenched *via* vibrational modes of the surface ligands than the NIR transitions of lanthanide ions like Yb, Er, Tm or Ho.

4 Conclusions

In conclusion, we studied the formation and the growth of Na$_{1.5-\frac{x}{2}}$Sr$_x$Gd$_{1.5-\frac{x}{2}}$F$_6$ nanocrystals for $0 \leq x \leq 1$. All particles were prepared by the reaction of ammonium fluoride with a solution of the metal oleates in oleic acid/octadecene. For $x \leq 0.2$, the reaction yields small ($\approx$3 nm) particles of the hexagonal phase β-Na$_{1.5-\frac{x}{2}}$Sr$_x$Gd$_{1.5-\frac{x}{2}}$F$_6$ already at 200 °C, whereas for larger values of x mainly small particles of the cubic phase α-Na$_{1.5-\frac{x}{2}}$Sr$_x$Gd$_{1.5-\frac{x}{2}}$F$_6$ are formed. In these cases, further heating at 320 °C dissolves the particles of the cubic phase and form larger particles of the hexagonal gagarinite phase. The final size of the β-Na$_{1.5-\frac{x}{2}}$Sr$_x$Gd$_{1.5-\frac{x}{2}}$F$_6$ particles as well as the time required for the conversion to the hexagonal phase strongly increases with increasing strontium content x, indicating that the presence of strontium hampers the formation of β-phase seeds. Full conversion is only observed for β-Na$_{1.5-\frac{x}{2}}$Sr$_x$Gd$_{1.5-\frac{x}{2}}$F$_6$ particles with $x \leq 0.75$. Particles with $x > 0.75$ can be prepared, however, *via* a core/shell type synthesis method: heating of β-Na$_{1.5-\frac{x}{2}}$Sr$_x$Gd$_{1.5-\frac{x}{2}}$F$_6$ particles with x = 0.75 together with a large amount of small α-NaGdSrF$_6$ particles (x = 1) at 320 °C results in almost complete dissolution of the α-phase particles and the growth of large α-Na$_{1.5-\frac{x}{2}}$Sr$_x$Gd$_{1.5-\frac{x}{2}}$F$_6$ particles with an average x-value close to one. The substitution of Na$^+$ and Gd^{3+} ions by Sr^{2+} ions increases the lattice parameters of the hexagonal phase. We observe a nearly linear increase of the lattice parameters of β-Na$_{1.5-\frac{x}{2}}$Sr$_x$Gd$_{1.5-\frac{x}{2}}$F$_6$ with x. For high values of x, the lattice parameters are similar to those of the hexagonal NaREF$_4$ phase of the lighter lanthanides (RE = Ce, Pr, Nd) and we could show that small α-NaGdSrF$_6$ particles (x = 1) can in fact be used as precursor to form a gagarinite shell on Tb^{3+} doped β-NaCeF$_4$ particles.

Conflicts of interest

There are no conflicts to declare.

Acknowledgements

References

1 F. Chen, W. Bu, S. Zhang, J. Liu, W. Fan, L. Zhou, W. Peng and J. Shi, *Adv. Funct. Mater.*, 2013, **23**, 298–307.

2 Y. Deng, H. Wang, W. Gu, S. Li, N. Xiao, C. Shao, Q. Xu and L. Ye, *J. Mater. Chem. B*, 2014, **2**, 1521–1529.

3 H. Guo, Z. Li, H. Qian, Y. Hu and I. N. Muhammad, *Nanotechnology*, 2010, **21**, 125602.

4 Y. Hou, R. Qiao, F. Fang, X. Wang, C. Dong, K. Liu, C. Liu, Z. Liu, H. Lei, F. Wang and M. Gao, *ACS Nano*, 2013, **7**, 330–338.

5 N. J. J. Johnson, W. Oakden, G. J. Stanisz, R. S. Prosser and F. C. J. M. van Veggel, *Chem. Mater.*, 2011, **23**, 3714–3722.

6 R. Naccache, P. Chevallier, J. Lagueux, Y. Gossuin, S. Laurent, L. Vander Elst, C. Chilian, J. A. Capobianco and M.-A. Fortin, *Adv. Healthcare Mater.*, 2013, **2**, 1478–1488.

7 H. Xing, S. Zhang, W. Bu, X. Zheng, L. Wang, Q. Xiao, D. Ni, J. Zhang, L. Zhou, W. Peng, K. Zhao, Y. Hua and J. Shi, *Adv. Mater.*, 2014, **26**, 3867–3872.

8 G. Chen, T. Y. Ohulchanskyy, S. Liu, W.-C. Law, F. Wu, M. T. Swihart, H. Agren and P. N. Prasad, *ACS Nano*, 2012, **6**, 2969–2977.

9 H. Groult, J. Ruiz-Cabello, J. Pellico, A. V. Lechuga-Vieco, R. Bhavesh, M. Zamai, E. Almarza, I. Martin-Padura, E. Cantelar, M. P. Martinez-Alcazar and F. Herranz, *Bioconjugate Chem.*, 2015, **26**, 153–160.

10 F. Li, C. Li, X. Liu, Y. Chen, T. Bai, L. Wang, Z. Shi and S. Feng, *Chem. – Eur. J.*, 2012, **18**, 11641–11646.

11 C. Liu, Z. Gao, J. Zeng, Y. Hou, F. Fang, Y. Li, R. Qiao, L. Shen, H. Lei, W. Yang and M. Gao, *ACS Nano*, 2013, **7**, 7227–7240.

12 C. Liu, Y. Hou and M. Gao, *Adv. Mater.*, 2014, **26**, 6922–6932.

13 C. Liu, W. Ma, Z. Gao, J. Huang, Y. Hou, C. Xu, W. Yang and M. Gao, *J. Mater. Chem. C*, 2014, **2**, 9637–9642.

14 J. Ryu, H.-Y. Park, K. Kim, H. Kim, J. H. Yoo, M. Kang, K. Im, R. Grailhe and R. Song, *J. Phys. Chem. C*, 2010, **114**, 21077–21082.

15 D. Vennerberg and Z. Lin, *Sci. Adv. Mater.*, 2011, **3**, 26–40.

16 F. Wang, D. Banerjee, Y. Liu, X. Chen and X. Liu, *Analyst*, 2010, **135**, 1839–1854.

17 J. Zhou, N. Shirahata, H.-T. Sun, B. Ghosh, M. Ogawara, Y. Teng, S. Zhou, R. G. S. Chu, M. Fujii and J. Qiu, *J. Phys. Chem. Lett.*, 2013, **4**, 402–408.

18 Y. Dai, H. Xiao, J. Liu, Q. Yuan, P. Ma, D. Yang, C. Li, Z. Cheng, Z. Hou, P. Yang and J. Lin, *J. Am. Chem. Soc.*, 2013, **135**, 18920–18929.

19 L. Wang, J. Liu, Y. Dai, Q. Yang, Y. Zhang, P. Yang, Z. Cheng, H. Lian, C. Li, Z. Hou, P. Ma and J. Lin, *Langmuir*, 2014, **30**, 13042–13051.

20 X. Wang, K. Liu, G. Yang, L. Cheng, L. He, Y. Liu, Y. Li, L. Guo and Z. Liu, *Nanoscale*, 2014, **6**, 9198–9205.

21 M. Yin, E. Ju, Z. Chen, Z. Li, J. Ren and X. Qu, *Chem. – Eur. J.*, 2014, **20**, 14012–14017.

22 K. Zarschler, L. Rocks, N. Licciardello, L. Boselli, E. Polo, K. P. Garcia, L. De Cola, H. Stephan and K. A. Dawson, *Nanomedicine*, 2016, **12**, 1663–1701.

23 S. E. Lohse and C. J. Murphy, *J. Am. Chem. Soc.*, 2012, **134**, 15607–15620.

24 J. Shen, Z. Li, R. Cheng, Q. Luo, Y. Luo, Y. Chen, X. Chen, Z. Sun and S. Huang, *ACS Appl. Mater. Interfaces*, 2014, **6**, 17454–17462.

25 B. M. van der Ende, L. Aarts and A. Meijerink, *Phys. Chem. Chem. Phys.*, 2009, **11**, 11081–11095.

26 C. Yuan, G. Chen, L. Li, J. A. Damasco, Z. Ning, H. Xing, T. Zhang, L. Sun, H. Zeng, A. N. Cartwright, P. N. Prasad and H. Agren, *ACS Appl. Mater. Interfaces*, 2014, **6**, 18018–18025.

27 K. Wang, J. Jiang, S. Wan and J. Zhai, *Electrochim. Acta*, 2015, **155**, 357–363.

28 W. J. Kim, M. Nyk and P. N. Prasad, *Nanotechnology*, 2009, **20**, 185301.

29 Y. Lu, J. Zhao, R. Zhang, Y. Liu, D. Liu, E. M. Goldys, X. Yang, P. Xi, A. Sunna, J. Lu, Y. Shi, R. C. Leif, Y. Huo, J. Shen, J. A. Piper, J. P. Robinson and D. Jin, *Nat. Photonics*, 2013, **8**, 32–36.

30 J. M. Meruga, A. Baride, W. Cross, J. J. Kellar and P. S. May, *J. Mater. Chem. C*, 2014, **2**, 2221–2227.

31 K. W. Krämer, D. Biner, G. Frei, H. U. Güdel, M. P. Hehlen and S. R. Lüthi, *Chem. Mater.*, 2004, **16**, 1244–1251.

32 M. M. Lage, R. L. Moreira, F. M. Matinaga and J.-Y. Gesland, *Chem. Mater.*, 2005, **17**, 4523–4529.

33 B. P. Sobolev, D. A. Mineev and V. P. Pashutin, *Dokl. Akad. Nauk SSSR*, 1963, **150**, 791–794.

34 A. Grzechnik, P. Bouvier, M. Mezouar, M. D. Mathews, A. K. Tyagi and J. Köhler, *J. Solid State Chem.*, 2002, **165**, 159–164.

35 J. H. Burns, *Inorg. Chem.*, 1965, **4**, 881–885.

36 O. V. Frank-Kamenetskaya, *Crystallogr. Rep.*, 1994, **39**, 923–928.

37 S. S. Perera, D. K. Amarasinghe, K. T. Dissanayake and F. A. Rabuffetti, *Chem. Mater.*, 2017, **29**, 6289–6297.

38 M. J. Sciberras, P. Leverett, P. A. Williams, D. E. Hibbs, A. C. Roberts and J. D. Grice, *Can. Mineral.*, 2011, **49**, 1111–1114.

39 A. A. Voronkov, *Zhurnal Struktumoi Khlmii*, 1962, **3**, 691–696.

40 X. Chen, D. Peng and F. Wang, *Nanomaterials*, 2013, **3**, 583–591.

41 L. Lei, D. Chen, P. Huang, J. Xu, R. Zhang and Y. Wang, *Nanoscale*, 2013, **5**, 11298–11305.

42 S. Zhao, W. Liu, X. Xue, Y. Yang, Z. Zhao, Y. Wang and B. Zhou, *RSC Adv.*, 2016, **6**, 81542–81551.

43 P. F. Zuo, S. L. Zhao, D. D. Song, B. Qiao, Z. Xu, J. J. Zhang, Q. X. Wu, P. J. Song and D. Gao, *J. Nanosci. Nanotechnol.*, 2018, **18**, 7584–7589.

44 J. Y. Dai, C. Yang, H. Zhang, G. Y. Feng and S. H. Zhou, *RSC Adv.*, 2017, **7**, 48238–48244.

45 L. Lei, D. Q. Chen, J. Xu, R. Zhang and Y. S. Wang, *Chem. – Asian J.*, 2014, **9**, 728–733.

46 L. Lei, J. A. Xia, Y. Cheng, Y. S. Wang, G. X. Bai, H. Xia and S. Q. Xu, *J. Mater. Chem. C*, 2018, **6**, 11587–11592.

47 X. W. Liu, Z. G. Yi, X. Qin, H. Liu, W. Huang and X. G. Liu, *Adv. Opt. Mater.*, 2019, **7**, 6.

48 Q. Q. Shao, H. Zhang, J. Y. Dai, C. Yang, X. X. Chen, G. Y. Feng and S. H. Zhou, *CrystEngComm*, 2019, **21**, 741–748.

49 X. F. Wang, Y. Wang, J. H. Yu, Y. Y. Bu and X. H. Yan, *Opt. Express*, 2018, **26**, 21950–21959.

50 Z. M. Xiong, Y. S. Yang and Y. F. Wang, *RSC Adv.*, 2016, **6**, 75664–75668.

51 A. H. Zhou, F. Song, Y. D. Han, F. F. Song, D. D. Ju and X. Q. Wang, *CrystEngComm*, 2018, **20**, 2029–2035.

52 Y. Zhang, Z. Yu, J. Li, Y. Ao, J. Xue, Z. Zeng, X. Yang and T. T. Tan, *ACS Nano*, 2017, **11**, 2846–2857.

53 Y. E. Serge Correales, C. Hazra, S. Ullah, L. R. Lima and S. J. L. Ribeiro, *Nanoscale Adv.*, 2019, **1**, 1936–1947.

54 M. M. A. Abualrejal, K. Eid, R. Tian, L. Liu, H. Chen, A. M. Abdullah and Z. Wang, *Chem. Sci.*, 2019, **10**, 7591–7599.

55 J. E. Choi, D. Kim and H. S. Jang, *Chem. Commun.*, 2019, **55**, 2261–2264.

56 H. Tang, H. Zhou and X. Cheng, *J. Lumin.*, 2020, **221**, 117086.

57 J. X. Zhao, X. Chen, B. Chen, X. Luo, T. Y. Sun, W. W. Zhang, C. J. Wang, J. Lin, D. Su, S. Qiao and F. Wang, *Adv. Funct. Mater.*, 2019, **29**, 1903295.

58 Z. Huang, Y. Yang, L. Gong, M. Ma and C. Xu, *Chem. Eng. J.*, 2016, **286**, 602–609.

59 G. F. Wang and Q. Peng, *J. Solid State Chem.*, 2011, **184**, 59–63.

60 F. Hund, *Z. Anorg. Chem.*, 1950, **261**, 106–115.

61 M. Ito, C. Goutaudier, Y. Guyot, K. Lebbou, T. Fukuda and G. Boulon, *J. Phys.: Condens. Matter*, 2004, **16**, 1501–1521.

62 M. Siebold, S. Bock, U. Schramm, B. Xu, J. L. Doualan, P. Camy and R. Moncorge, *Appl. Phys. B: Lasers Opt.*, 2009, **97**, 327–338.

63 P. J. Bendall, C. R. A. Catlow, J. Corish and P. W. M. Jacobs, *J. Solid State Chem.*, 1984, **51**, 159–169.

64 R. E. Thoma, *Inorg. Chem.*, 1966, **5**, 1222–1229.

65 P. P. Fedorov, *Russ. J. Inorg. Chem.*, 1999, **44**, 1703–1727.

66 T. Rinkel, J. Nordmann, A. N. Raj and M. Haase, *Nanoscale*, 2014, **6**, 14523–14530.

67 T. Rinkel, A. N. Raj, S. Dühnen and M. Haase, *Am. Ethnol.*, 2016, **128**, 1177–1181.

68 B. Voss and M. Haase, *ACS Nano*, 2013, **7**, 11242–11254.

69 C. Homann, L. Krukewitt, F. Frenzel, B. Grauel, C. Wurth, U. Resch-Genger and M. Haase, *Angew. Chem., Int. Ed.*, 2018, **57**, 8765–8769.

70 A. Naduviledathu Raj, T. Rinkel and M. Haase, *Chem. Mater.*, 2014, **26**, 5689–5694.